5780 *Chem. Mater.* **2010,** *22,* 5780–5785
DOI:10.1021/cm101940u

CHEMISTRY OF MATERIALS
Article

Nanoscale Control of Silica Particle Formation via Silk−Silica Fusion Proteins for Bone Regeneration

Aneta J. Mieszawska,[†] Lauren D. Nadkarni,[†] Carole C. Perry,[‡] and David L. Kaplan*[,†]

[†]*Department of Biomedical Engineering, Tufts University, Medford, Massachusetts 02155, United States, and* [‡]*School of Science and Technology, Nottingham Trent University, Nottingham NG11 8NS, United Kingdom*

Received July 12, 2010

The biomimetic design of silk/silica fusion proteins was carried out, combining the self-assembling domains of spider dragline silk (*Nephila clavipes*) and the silaffin-derived R5 peptide of *Cylindrotheca fusiformis* that is responsible for silica mineralization. Genetic engineering was used to generate the protein-based biomaterials, incorporating the physical properties of both components. With genetic control over the nanodomain sizes and chemistry, as well as modification of synthetic conditions for silica formation, controlled mineralized silk films with different silica morphologies and distributions were successfully generated as three-dimensional (3D) porous networks, clustered silica nanoparticles (SNPs), or single SNPs. Silk serves as the organic scaffolding to control the material stability, and multiprocessing makes silk/silica biomaterials suitable for different tissue regenerative applications. The influence of these new silk−silica composite systems on osteogenesis was evaluated with human mesenchymal stem cells (hMSCs) subjected to osteogenic differentiation. hMSCs adhered, proliferated, and differentiated toward osteogenic lineages on the silk/silica films. The presence of the silica in the silk films influenced osteogenic gene expression, with the upregulation of alkaline phosphatase (ALP), bone sialoprotein (BSP), and collagen type 1 (Col I) markers. Evidence for early bone formation as calcium containing deposits was observed on silk films with silica. These results indicate the potential utility of these new silk/silica systems toward bone regeneration.

Introduction

Biomaterials with tunable nanoscale features can offer improved performance for in vivo applications.[1] Silica is widely used in industry, medicine, and nanotechnology applications where structural control is necessary but also challenging.[2,3] Here, we describe a new procedure using ambient conditions, for the unusual and detailed control of silica morphology and distribution on the surface of silk films utilizing genetically engineered chimeric proteins. A genetic combination of spider dragline silk sequence (*Nephila clavipes*) and the silaffin-derived R5 peptide of the diatom (*Cylindrotheca fusiformis*) led to the bioinspired synthesis of 3D porous silica networks, clustered silica nanoparticles (SNPs), or single/isolated SNPs. We anticipate that these silica-based biomaterials will have applications in tissue regeneration and drug delivery, because of the ability to regulate the location and morphological features of the silica. The silk component serves as an organic scaffold that controls material stability and allows multiple modes of processing. Silica serves as an important osteoinductive element with potential control of remodeling rate and tissue regeneration outcomes in vivo. In addition, silicon-derived nanostructures with strong morphological and spatial control are attractive for use in electronics,[4] biosensors,[5] microfluidic devices,[6] and DNA microarray technology.[7] The novelty in material design also allows for applications in biodopants[8] and protein−silica nanocomposites.[9]

Silica biomineralization has attracted much attention, because of the remarkable morphological control of silica nanopatterns synthesized *in vivo* that exceed current synthetic and technological capabilities *in vitro*. Examples of controlled silica biosynthesis are the skeletal architectures from diatoms formed under physiological conditions (aqueous environment, neutral pH, low temperatures) and driven by biomolecules,[10,11] in contrast with harsh industrial synthesis conditions. Studies to date show widespread bioapplications of porous silica nanostructures in

*Author to whom correspondence should be addressed. E-mail: David.Kaplan@tufts.edu.

(1) Sakiyama-Elbert, S. E.; Hubbell, J. A. *Annu. Rev. Mater. Res.* **2001**, *31*, 183–201.
(2) Tan, W.; Wang, K.; He, X.; Zhao, X. J.; Drake, T.; Wang, L.; Bagwe, R. P. *Med. Res. Rev.* **2004**, *24*, 621–638.
(3) Coradin, T.; Livage, J. *Acc. Chem. Res.* **2007**, *40*, 819–826.
(4) Neaton, J. B.; Muller, D. A.; Ashcroft, N. W. *Phys. Rev. Lett.* **2000**, *85*, 1298–1301.
(5) Kilian, K. A. B.; Gooding, T. J. *Chem. Commun.* **2009**, *6*, 630–640.
(6) Yeung, E. S. *Annu. Rev. Phys. Chem.* **2004**, *55*, 97–126.
(7) Ramana Murthy, B.; Ng, J. K. K.; Selamat, E. S.; Balasubramanian, N.; Liu, W. T. *Biosens. Bioelectron.* **2008**, *24*, 723–728.
(8) Silver, J.; Withnall, R.; Ireland, T. G.; Fern, G. R.; Zhang, S. *Nanotechnology* **2008**, *19*, 095302/1–095302/7.
(9) Ramanathan, M.; Luckarift, H. R.; Sarsenova, A; Wild, J. R.; Ramanculov, E. K.; Olsen, E. V.; Simonian, A. L. *Colloids Surf. B* **2009**, *73*, 58–64.
(10) Sumper, M.; Brunner, E. *ChemBioChem* **2008**, *9*, 1187–1194.
(11) Perry, C. C.; Keeling-Tucker, T. *J. Biol. Inorg. Chem.* **2000**, *5*, 537–550.

Published on Web 09/22/2010

drug delivery,[12] targeted therapies,[13] and cell labeling, where internalization shows no cytotoxic effects.[14] Silica can also be easily derivatized to immobilize antibodies or proteins, and once supported on a stable scaffold carrier, they can be excellent implant materials. Silica nanoparticles enhance and stabilize the fluorescence of encapsulated organic dyes[15] and, when bioconjugated, find applications in imaging, sensing, targeting, and detection of single cells. Also, inorganic−organic silica hybrids have potential use in optoelectronics,[16] molecular machines,[17] tunable lasers,[18] or electrodes for biofuel cells.[19]

Silica nanostructures of different morphologies and distributions synthesized on silk films have not been previously fabricated. Other bioinspired silica particle formation,[20] as well as silica structures with different morphologies (arch shapes, fibers),[21] have appeared. The present work represents a new type of biomaterial with many benefits. First, silk/silica binding chimeric proteins precipitate silica in situ,[22] at room temperature with commercially available reagents, without the need for specialized equipment. Second, silks self-assemble into highly stable β-sheet structures[23] with remarkable mechanical properties that improve material properties and stability against organic solvents, water, and strong acids and bases. Third, the biodegradability of silk[24] and the aqueous processing conditions for silica mineralization make it suitable for use in living tissues. Furthermore, since the sizes and distributions of the silica component can be controlled in the bioengineering process, new levels of control of degradation lifetime can be tailored into the materials. Fourth, silks can be processed into fibers,[25] films,[26] porous matrices,[27] or hydrogels.[28] Finally, surfactant-free silica nanostructures offer silanol groups that can be utilized for a diverse range of applications.

(12) Radu, D. R.; Lai, C.-Y.; Jeftinija, S.; Lin, V. S.-Y. *J. Am. Chem. Soc.* **2004**, *126*, 13216–13217.
(13) Lu, J. L., M.; Sherman, S.; Xia, T.; Kovochich, M.; Nel, A. E.; Zink, J. I.; Tomanoi, F. *Nanobiotechnology* **2007**, *3*, 89–95.
(14) Lin, Y.; Tsai, C.-P.; Huang, H.-Y.; Kuo, C.-T.; Hung, Y.; Huang, D.-M.; Chen, Y.-C.; Mou, C.-Y. *Chem. Mater.* **2005**, *17*, 4570–4573.
(15) MacCraith, B. D.; McDonagh, C. *J. Fluoresc.* **2002**, *12*, 333–342.
(16) Innocenzi, P.; Lebeau, B. *J. Mater. Chem.* **2005**, *15*, 3821–3831.
(17) Angelos, S.; Johansson, E.; Stoddart, J. F.; Zink, J. I. *Adv. Funct. Mater.* **2007**, *17*, 2261–2271.
(18) Reisfeld, R.; Weiss, A.; Saraidarov, T.; Yariv, E.; Ishchenko, A. A. *Polym. Adv. Technol.* **2004**, *15*, 291–301.
(19) Lim, J.; Malati, P.; Bonet, F.; Dunn, B. *J. Electrochem. Soc.* **2007**, *154*, A140–A145.
(20) Steinmetz, N. F.; Shah, S. N.; Barclay, J. E.; Rallapalli, G.; Lomonossoff, G. P.; Evans, D. J. *Small* **2009**, *5*, 813–816.
(21) Rodriguez, F.; Glawe, D. D.; Naik, R. R.; Hallinana, K. P.; Stone, M. O. *Biomacromolecules* **2004**, *5*, 261–265.
(22) Foo, C. W. P.; Patwardhan, S. V.; Belton, D. J.; Kitchel, B.; Anastasiades, D.; Huang, J.; Naik, R. R.; Perry, C. C.; Kaplan, D. L. *Proc. Natl. Acad. Sci. U.S.A.* **2006**, *103*, 9428–9433.
(23) Matsumoto, A.; Chen, J.; Collette, A. L.; Kim, U.-J.; Altman, G. H.; Cebe, P.; Kaplan, D. L. *J. Phys. Chem. B* **2006**, *110*, 21630–21638.
(24) Li, M.; Ogiso, M.; Minoura, N. *Biomaterials* **2003**, *24*, 357–365.
(25) Jin, H.-J.; Fridrikh, S. V.; Rutledge, G. C.; Kaplan, D. L. *Biomacromolecules* **2002**, *3*, 1233–1239.
(26) Jin, H. J.; Park, J.; Karageorgiou, V.; Kim, U.-J.; Valluzzi, R.; Cebe, P.; Kaplan, D. L. *Adv. Func. Mater.* **2005**, *15*, 1241–1247.
(27) Kim, H. J.; Kim, U. J.; Vujnak-Novakovic, G.; Min, B. H.; Kaplan, D. L. *Biomaterials* **2005**, *26*, 4442–4452.
(28) Kim, U. J.; Park, J. Y.; Li, C. M.; Jin, H. J.; Valluzzi, R.; Kaplan, D. L. *Biomacromolecules* **2004**, *5*, 786–792.

The objective of the current study was to design, clone, and express a new family of silk−silica fusion proteins, wherein silica morphology and distribution could be controlled to a high degree, and osteogenesis would be promoted from stem cells.

Experimental Section

Chemicals. All chemicals were purchased from Sigma−Aldrich (St. Louis, MO, USA) or Fluka (Milwaukee, WI, USA) and used without further purification. Cell medium ingredients were purchased from Invitrogen (Carlsbad, CA, USA) and Sigma−Aldrich.

Preparation of Silk/Silica Chimeric Proteins. Silk/silica chimeric proteins were genetically engineered and expressed using our previous procedure.[22] Expressed proteins were purified using Ni-NTA resin (Qiagen, Valencia, CA, USA) and dialyzed (membrane MWCO 2000 g mol^{-1}; Pierce, Woburn, MA, USA) in a 100 mM phosphate buffer at pH 5.5 for 1 day, changing buffer 2 times, and against distilled water for 3 days, changing the water 3 times a day. The silk solutions were freeze-dried to obtain the protein powder.

Preparation of Silk and Silk/Silica Films. Hexafluoro-2-propanol (HFIP)-based silk solutions were prepared at a concentration of 2.5% and 5% wt/vol and stirred overnight to ensure complete protein dissolution. Next, 50 μL of the silk solutions were cast on the bottom of polystyrene boat used subsequently for scanning electron microscopy (SEM) imaging and 24-well tissue culture plate (TCP) used for cell culture. Films were left to dry for 24 h. Next, 2 mL of 90% methanol solution in water was added to each boat and incubated for 10 min to induce β-sheet formation in the silk films. Next, the 2.5 and 5% silk films were soaked in 2 mL of 5.5 mM phosphate buffer for 30 min. After that, 200 μL of mineralizing solution containing prehydrolysed tetramethyl orthosilicate (TMOS) was added to the phosphate buffer and films were incubated for 1 h to form silica deposits on silk film surface. Also, 2.5% silk films in phosphate buffer were treated with 500 μl of mineralizing solution containing glycerol (99%) at 60% vol/vol. All films were rinsed well with ultrapure water and dried in air. Methanol was then removed and films were left to dry overnight in a fume hood. This step was used to generate silk films that were stable in an aqueous environment and suitable for cell culture. Films were sterilized with 70% ethanol, left to dry, and placed under UV light for 5 min in a laminar flow hood. TCP only was used as a control. Prior to cell seeding, 1 mL of cell culture medium was added to each well, soaked for 30 min, and then aspirated.

Human Mesenchymal Stem Cells (hMSCs). Bone marrow aspirate from a young healthy donor was obtained from Lonza (Walkersville, MD). Frozen low-passage (2 or 3) human mesenchymal stem cell (hMSC) stocks were thawed and suspended in a growth medium containing high-glucose Dulbecco's modified eagle medium (DMEM) supplemented with 10% fetal bovine serum, 1% antibiotic/antimycotic, 1% nonessential amino acids, and 10 ng of basic fibroblast growth factor (bFGF). The cells were plated onto the silk and silk/silica films at a density of 5000 cells/well in a 24-well plate and kept in a humidified incubator at 37 °C and 5% CO_2. The cells were cultured in hMSC media until 85% confluency, and then the medium was changed to an osteogenic medium containing high-glucose DMEM supplemented with 10% fetal bovine serum, 1% antibiotic/antimycotic, 1% nonessential amino acids, 100 nM dexamethasone, 10 mM β-glycerolphosphate, and 0.05 mM L-ascorbic acid 2-phosphate. The medium was changed every

Scheme 1. Method To Control Silica Distribution on Silk Films

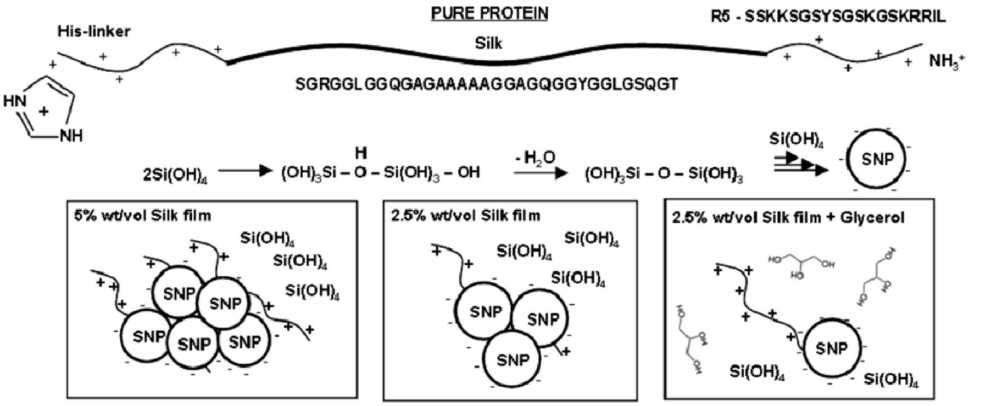

3−4 days. Cell growth and shape were monitored using a phase-contrast light microscope (Carl Zeiss, Jena, Germany) equipped with a Sony Exwave HAD 3CCD (Sony Electronics, Inc., USA) color video camera.

Gene Expression Using Real-Time RT-PCR Analysis. After osteogenic culture, the cells from three separate wells of each type were lysed in 0.35 mL Buffer RLT (Qiagen No. 79216, Valencia, CA, USA) containing 10% mercaptoethanol, followed by shredding in a QIAshedder (Qiagen No. 79656). RNA was isolated from the cells using an RNeasy Mini Kit (Qiagen No. 74106). From this RNA, cDNA was synthesized using a High Capacity cDNA Reverse Transcription Kit (Applied Biosystems No. 4368814, Framingham, MA, USA), following the manufacturer's instructions. The cDNA samples were analyzed for expression of alkaline phosphatase, collagen type I, and bone sialoprotein, relative to the GAPDH housekeeping gene, using Assay-on-Demand Gene Expression kits with TaqMan Universal PCR Master Mix (ABI #4364340, Applied Biosystems AoD probes, Framingham, MA, USA). The data were analyzed using the ABI Prism 7000 Sequence Detection Systems software.

SEM Characterization Parameters. After 2 weeks of osteogenic culture, the basal parts of the tissue culture dishes were removed and fixed in 2.5% vol/vol glutaraldehyde solution in phosphate-buffered saline (PBS) for 30 min. Next, the samples were washed in deionized water (DI) water and dehydrated via 20 min of incubation in a series of ethanol-in-water solutions (10%, 30%, 60%, 80%, 90%, 100% vol/vol). Surface morphology down to the nanometer levels was evaluated using a Carl Zeiss (Carl Zeiss SMT, Germany) Ultra 55 field emission scanning electron microscopy (FESEM) system operating at an accelerating voltage of 10 kV and using an in-lens ion annular secondary electron detector. The bottom of the tissue culture plate (TCP) well with cast film was cut and coated with a carbon layer (Baltec Carbon Coater, model MED-020, Liechtenstein) to ensure sample conductivity necessary for imaging. Elemental composition of the silk film surface was evaluated using an energy-dispersive X-ray analysis (EDAX) spectrometer that was connected to the SEM instrument.

Results and Discussion

Scheme 1 shows the strategy for biomaterial formation and mineralization method that led to three types of silk/silica surfaces. Five percent (5%) and 2.5% wt/vol silk films produce two different morphologies of silica deposits: a three-dimensional (3D) dense network and aggregates of SNPs distributed over the silk surface,

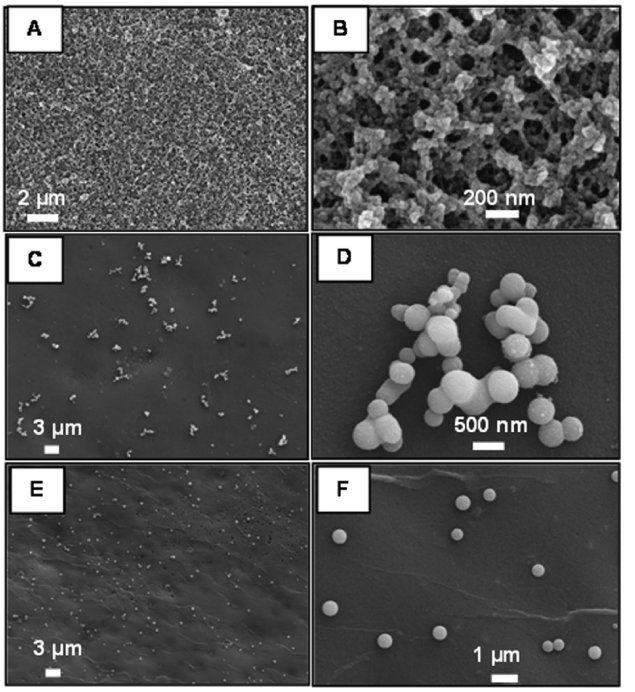

Figure 1. SEM images of (A,B) 5%, (C,D) 2.5%, and (E,F) 2.5% (glycerol) wt/vol silk films with silica nanostructures.

respectively. Silica was deposited on the silk film surface presumably through electrostatic interactions of negatively charged silica species and the R5 peptide.[22] The additional positive charge on the silk surface was induced via charged imidazole groups of the N-terminal histidine tag, which enhanced silica deposition.[29,30] Also, 2.5% silk films produced dispersed SNPs on the silk film surface when glycerol was present in the mineralizing solution. The addition of glycerol aids in the dispersion of SNPs on the silk film surface, likely through stabilization of SNPs, thus preventing aggregation. Figure 1 compares silica morphologies and distribution on the surface of silk films formed under the different conditions. Figures 1A and 1B show SEM images of a 5% silk film after the silicification reaction. The surface exhibits silica nanostructures

(29) Belton, D. J.; Patwardhan, S. V.; Perry, C. C. *Chem. Commun.* **2005**, *27*, 3475–3477.
(30) Liang, M. K.; Patwardhan, S. V.; Danilovtseva, E. N.; Annekov, V. V.; Perry, C. C. *J. Mater. Res.* **2009**, *24*, 1700–1708.

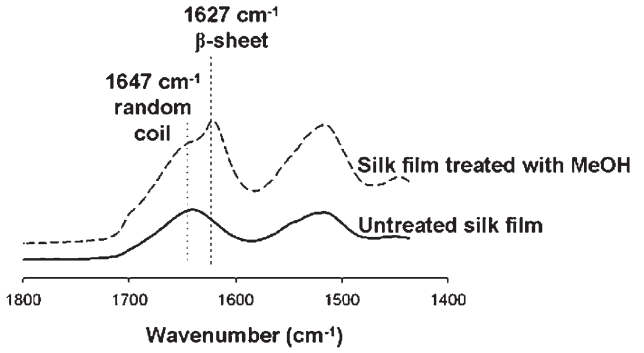

Figure 2. Comparison of FTIR spectra of silk film before and after methanol treatment. Methanol induces β-sheet formation within the silk film, as shown by a shift in the Fourier transform infrared (FTIR) spectrum.

arranged in dense 3D networks, consistent with the model in Scheme 1. The abundance of positive charges expected for 5% silk films induces a strong attraction for silica species to the surface of the silk film, causing the immediate precipitation of silica that uniformly covers the entire silk film surface. The high microporosity of the silica deposits increases the amount of surface hydroxyl groups that can be functionally modified, forming new inorganic−organic hybrids. This type of material can become compatible in various solutions and is currently being examined for its potential as a drug delivery vehicle. Figures 1C and 1D show SEM images of SNPs precipitated on a 2.5% silk film surface. The surface contains a lower overall density of silica nanostructures (2.4 μm^{-2}), as compared to 100% coverage discussed above, and, more importantly, the silica morphology changed drastically with predominant clusters of SNPs, compared to the widespread porous network observed for the 5% silk films. The average diameter of SNPs is fairly uniform (400 $\pm$ 90 nm). The decreased concentration of silk reduces the overall content of R5 peptide and histidine moieties on the film surface, which leads to localized distribution of positive charges and local precipitation of SNPs. The addition of glycerol to the silicification reaction on 2.5% silk films changes the SNP distribution on the surface of silk films, as shown in Figures 1E and 1F. The surface is covered with uniformly spread isolated SNPs with a density of 1.6 μm^{-2}. The nanometer size range and separation of SNPs over large areas offers unique properties of this biomaterial, with respect to applications in tissue engineering. The surfactant-free SNP surfaces can be easily modified for targeted therapies or for imaging.

The effect of methanol treatment on silk films was evaluated to induce a structural transition from random coil to secondary β-sheet structure,[31] which is the stable protein conformation in an aqueous environment. The tendency of the films to form β-sheets can be evaluated using Fourier transform infrared (FTIR) spectroscopy by analyzing amide I (1600−1700 cm^{-1}) and amide II (1500−1600 cm^{-1}) regions of the silk film spectrum, as shown in Figure 2. The characteristic peak at 1627 cm^{-1} corresponds to the N−H stretch and indicates hydrogen bond and β-sheet formation within the film, after solvent treatment.

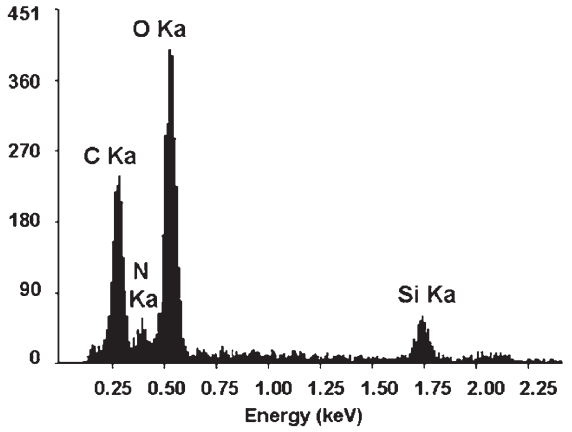

Figure 3. EDAX spectrum of silk/silica film exhibiting strong peaks for elemental silicon and oxygen, which confirm that nanostructures observed on the surface of silk film originate from silica.

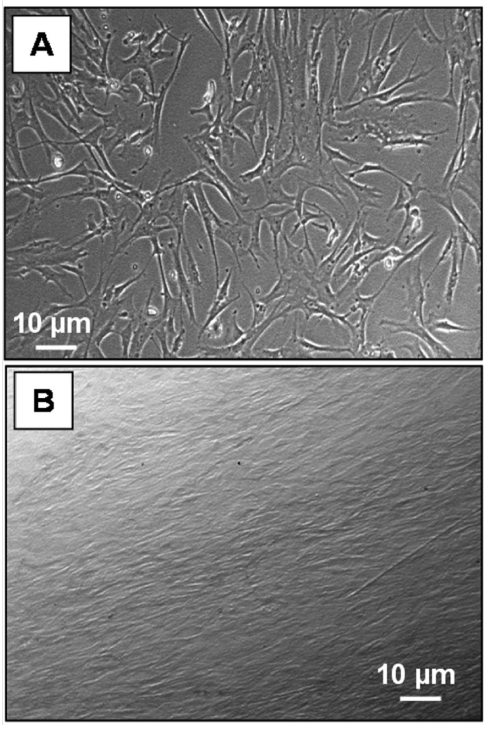

Figure 4. Optical microscopy images of hMSCs on 5% wt/vol silk films mineralized with silica (A) before and(B) after differentiation into osteogenic lineages.

The silica formation on silk/silica films was confirmed by EDAX analysis, and a representative spectrum is shown in Figure 3. The presence of silicon and oxygen peaks at 1.74 and 0.623 keV, respectively, indicate that the nanostructures observed in SEM images (Figure 1) originate from silica. The oxygen content is partially attributed to the underlying silk film, as well as carbon (also coating) and nitrogen.

Enhancement of new bone formation with silica-containing bone implants has already been established. Nevertheless, the use of nanostructural silica in a supporting

(31) Murphy, A. R.; St. John, P.; Kaplan, D. L. *Biomaterials* **2008**, *29*, 2829–2838.

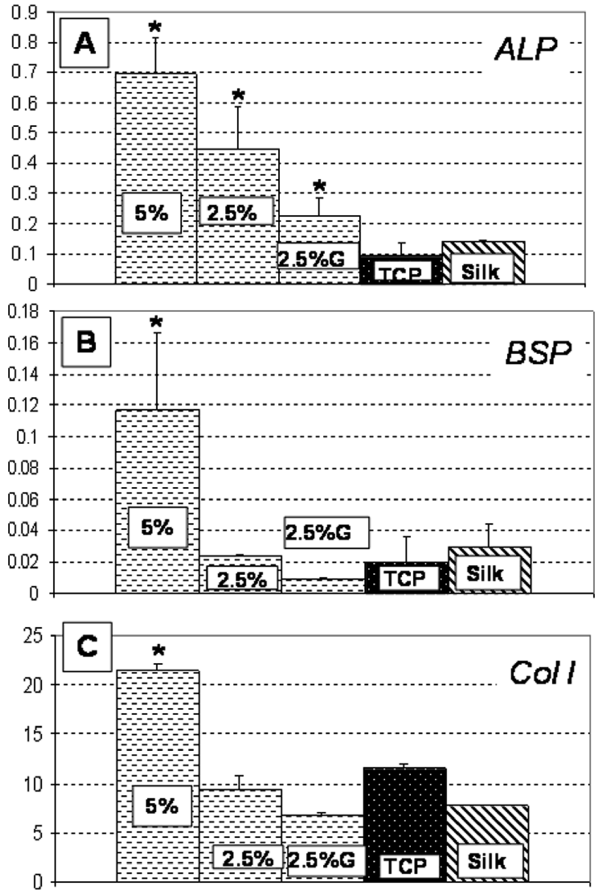

Figure 5. Osteogenic gene expression of cells grown on 5% wt/vol silk films with silica or silk only (denoted as "Silk") and tissue culture plastic (denoted as "TCP") after exposure to osteogenic stimulants for 2 weeks: (A) alkaline phosphatase (ALP), (B) bone sialoprotein (BSP), and (C) collagen I (Col I). Each column represents the mean and standard deviation of $N = 3$ independent cultures. $P < 0.05$.

matrix is often desired to enable material biodegradation within appropriate time frames, matching the rates of new bone tissue formation. It was also shown that primary human osteoblasts adhere better to roughened mineral surfaces.[32] We tested our silk/silica films to support the hMSC growth and osteogenic differentiation. Control samples were silk film only without silica mineralization and TCP. Cells showed good adhesion to all silk/silica films and proliferation rates reaching 85% confluence on day 5, the starting point of osteogenic differentiation. Cells grown on plastic reached 95% confluence on day 5, showing similar growth rates. Cell morphology was examined by light microscopy at two time points: 5 days after cell seeding and 2 days after differentiation into osteogenic lineage. Before differentiation, similar cell densities and morphologies were observed on all silk films, showing spindle-like shapes characteristic of undifferentiated fibroblastic hMSCs, with an example morphology shown in Figure 4A. After 2 days of osteogenic stimulation, cells spread evenly on silk film surfaces, forming a thin coating with closely packed flattened cells, as can be observed in a representative image in Figure 4B. No differences in cell morphology

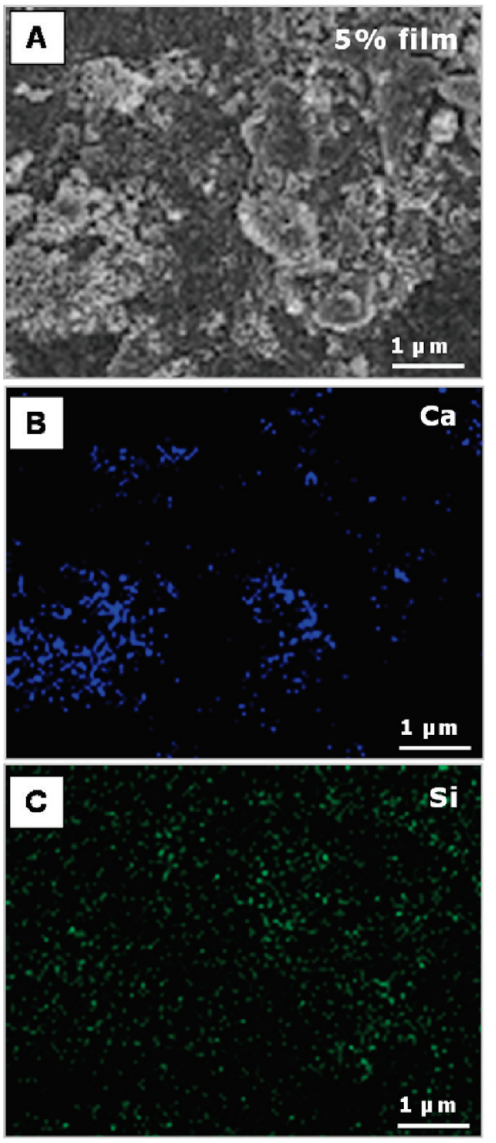

Figure 6. SEM image and EDAX mapping of 5% wt/vol silk film with silica after 2 weeks of hMSC osteogenic culture.

were observed between the silk/silica samples and the control samples, although after 2 weeks of osteogenic culture, some detachment and cell clustering was observed for cells grown on TCP and silk only but not on silk/silica films.

The ability of silica dissolution ions to enhance new bone formation has already been established with bioactive glasses commonly used as bone implants.[33,34] We further evaluated silk/silica films for the ability to modulate hMSC differentiation. Expression of bone-specific markers was quantified using real-time RT-PCR after 2 weeks of osteogenic culture. Figure 5A shows that alkaline phosphatase was upregulated on all silk/silica films, with respect to the control samples (silk only and TCP). Figure 5B shows that bone sialoprotein (BSP) gene expression was upregulated when the cells were cultured

(32) Gough, J. E.; Notingher, I.; Hench, L. L. *J. Biomed. Mater. Res., Part A* **2004**, *68*, 640–650.
(33) Christodoulou, I.; Buttery, L. D. K.; Tai, G.; Hench, L. L.; Polak, J. M. *J. Biomed. Mater. Res., Part B* **2006**, *77B*, 431–446.
(34) Bombonato-Prado, K. F.; Bellesini, L. S.; Junta, C. M.; Marques, M. M.; Passos, G. A.; Rosa, A. L. *J. Biomed. Mater. Res., Part A* **2008**, *88*, 401–408.

on 5% silk films mineralized with silica, with respect to the control samples. Expression of collagen I also was elevated on 5% silk films mineralized with silica in osteogenic culture, when compared to the controls. The upregulation of ALP on all silk/silica films, BSP and Col 1 on 5% silk/silica film in osteogenic culture suggests the influence of silica's presence on gene expression toward upregulation of osteogenesis. Also, since BSP upregulation is an indication of early apatite nucleation,[35] we further tested 5% silk/silica film with EDAX mapping to evaluate the calcium presence. After 2 weeks in osteogenic cell culture, we observed calcium mineral deposits on 5% silk/silica film surface (Figure 6), which is the main component of early apatite. The silicon signal was also observed, indicating residual silica minerals.

Conclusions

A method to control silica deposition on the surface of stable silk films was demonstrated. Different mineral phase loading and morphologies can be tailored synthetically, thus altering the biomaterial properties. The size scale, the all-aqueous conditions, and room-temperature processing offer in situ reactions in tissue-compatible environments to replace currently used bulk silica or bioactive glasses, as well as benefits for imaging and delivery.[36] Bioengineering offers fine control over the protein design, in terms of nanodomain size, chemistry, and morphology to regulate the biomaterial properties. This approach can be extended to introduce alternative fusions of inorganic phases for other applications. Preliminary studies with human mesenchymal stem cells (hMSCs) show support of silk/silica films toward cell attachment and upregulation of osteogenic gene markers, the latter pronounced highly on 5% silk film with porous silica network. These results indicate that silk/silica system enhances osteogenesis.

Acknowledgment. This research was supported by NIH (DE017207) and AFOSR (FA 9550-07-1-0079). This work was performed in part at the Center for Nanoscale Systems (CNS), a member of the National Nanotechnology Infrastructure Network (NNIN), which is supported by the National Science Foundation under NSF Award No. ECS-0335765. CNS is part of the Faculty of Arts and Sciences at Harvard University. C.C.P. acknowledges additional financial support from EPSRC EP/E048439/1.

(35) Gordon, J. A.; Tye, C. E.; Sampaio, A. V.; Underhill, T. M.; Hunter, G. K.; Goldberg, H. A. *Bone* **2007**, *41*, 462–473.
(36) Boccaccini, A. R.; Notingher, I.; Maquet, V.; Jerome, R. *J. Mater. Sci. Mater. Med.* **2003**, *14*, 443–450.